Comparison of detailed experimental wavenumber spectra with gyrokinetic simulation aided by two-dimensional full-wave simulations

T. Happel,[1,*] T. Görler,[1] P. Hennequin,[2] C. Lechte,[3] M. Bernert,[1] G.D. Conway,[1]
S. J. Freethy,[1,4] C. Honoré,[2] J. Pinzón,[1] U. Stroth,[1,5] and the ASDEX Upgrade Team[1]

[1]*Max-Planck-Institut für Plasmaphysik, Boltzmannstr. 2, 85748 Garching, Germany*

[2]*Laboratoire de Physique des Plasmas,*
Ecole Polytechnique, 91128 Palaiseau, France

[3]*IGVP, Universität Stuttgart, Pfaffenwaldring 31, 70569 Stuttgart, Germany*

[4]*Plasma Science and Fusion Center, Massachusetts Institute of Technology,*
Cambridge, Massachusetts 02139, USA

[5]*Physik-Department E28, Technische Universität München,*
James-Franck-Str. 1, 85748 Garching, Germany

(Dated: 2017-03-02)

Abstract

The importance of using a comprehensive suite of tools for the validation of a gyrokinetic code is described. This is detailed by presenting experimental wavenumber spectra which show pronounced differences, although they are measured at the same toroidal, poloidal and radial location. They are obtained via Doppler reflectometry and the differences are due to the probing beam polarization. These differences are reproduced convincingly using turbulence from a gyrokinetic simulation as input for two-dimensional full-wave simulation. It is demonstrated that the application of synthetic diagnostics is indispensable if non-trivial diagnostics are used in the experiment. Furthermore, the measurement of wavenumber spectra via Doppler reflectometry with X-mode probing beam polarization might be problematic due to nonlinear wave-plasma interactions and should be regarded with care when used for quantitative statements or the validation of gyrokinetic codes.

PACS numbers: 52.35.Ra, 52.55.Fa, 52.70.Gw, 52.25.Os

*Electronic address: tim.happel@ipp.mpg.de

I. INTRODUCTION

A profound understanding of plasma turbulence is of major importance for magnetically confined fusion plasma research and projections toward next-step fusion devices such as ITER or DEMO. Since turbulence impacts the transport properties of a fusion plasma, it is a key player for determining the energy and particle fluxes and thus dictates the shape of the final density and temperature profiles, which – together – set the confinement and thus the efficiency of the fusion reactor.

Hence, not only for the understanding and interpretation of observations from today's magnetically confined plasmas, but also for predictions for future devices, numerical simulations have become one of the most important tools. While the verification of the mathematical validity of codes is in an advanced state today [1–6], a careful validation including turbulence measurements and their comparison to nonlinear simulations, is an ongoing effort. [7–17].

Fluctuation wavenumber spectra contain a variety of information about underlying linear microinstabilities and energy transfer mechanisms. In magnetic confinement fusion research, typically two-dimensional (2D) turbulence is observed due to the strong anisotropy in perpendicular and parallel directions to the magnetic field, $k_\perp \gg k_\parallel$ [18]. In a simple, yet instructive 2D neutral-fluid Navier stokes turbulence picture, energy is injected into a 2D system at a spatial scale k_i. The "pool", into which energy can be distributed, is determined by the boundaries set by the system size k_sys at large scales and by the dissipation scale k_diss at small scales, such that for standard considerations $k_\mathrm{sys} < k_\mathrm{i} < k_\mathrm{diss}$ holds. In this simple picture, the initially energy-free scales between the characteristic scales are called *inertial* ranges. As energy is injected into the system, it is transferred toward k_sys (energy cascade or *inverse* cascade) and k_diss (enstrophy cascade). The efficiencies of these cascades differ for neutral-fluid Navier-Stokes turbulence, such that the inertial ranges can be characterized by different spectral indices. For a review on 2D turbulence and wavenumber spectra, see Ref. [19].

However, different from neutral-fluid Navier-Stokes turbulence, in magnetic confinement fusion research, several species (ions, electrons, impurities) are fluctuating, which interact due to their charges, in a magnetic field which can also become fluctuating. The dimensionality of plasma turbulence is higher than in Navier-Stokes turbulence. Hence, dissipation channels and cascades can also exist in velocity space. Furthermore, more than one energy injection scale can exist if several unstable modes are present. It is thus not surprising that the simple neutral-fluid

picture is not expected to carry over exactly to the wavenumber spectra of a magnetic confinement fusion experiment. In fact, several theories have been put forward that result in a variety of spectral indices. These theories are based on many different mechanisms such as nonlinear phase mixing [20], three-dimensional effects [21], nonlinear energy transfer into damped eigenmodes [22], disparate scale interactions (non-local in k-space) [23], predator-prey dynamics [24], or the coexistence of dissipation or damping and turbulence drive [25, 26]. The wavenumber spectrum of a magnetic confinement fusion experiment has many degrees of freedom, and it is a very challenging (and potentially very rewarding) task to validate gyrokinetic simulations through wavenumber spectra [27]. It is important to stress that heat fluxes, which are normally used to consider whether a gyrokinetic simulation describes an experimental situation sufficiently well, are 1D quantities and as such much less stringent than the wealth of information obtained when measuring a wavenumber spectrum. Note that research into wavenumber spectra and validation of gyrokinetic simulations is also an active field in astrophysical plasma research [28–30].

The fluctuation wavenumber spectrum can be measured with a variety of diagnostics; the most direct measurement is based on wave scattering [31–36]. Another advanced method is Upper Hybrid Resonance backscattering [37]. This work concentrates on the wavenumber-resolved measurement of density turbulence, obtained with Doppler reflectometry (also called Doppler backscattering) [38, 39]. By scanning the perpendicular wavenumber of density fluctuations, this diagnostic is suited to measure wavenumber spectra [38, 40–53]. However, it has been pointed out that the validity of turbulence amplitude measurements could be affected by the microwave polarization. In particular, for a given density gradient length, theory predicts that nonlinear effects are encountered for X-mode polarization at lower turbulence levels than for O-mode polarization [54, 55]. Since the diagnostic response can be linear, nonlinear, or even saturated, it is indispensable to use a reliable synthetic diagnostic for validation studies. In the present paper, this is done via 2D full-wave analysis, which has been applied since more than a decade to study the complex plasma-wave interactions pertaining to Doppler reflectometer measurements [56–61].

Experiments have been conducted on the ASDEX Upgrade tokamak (AUG). The experimental wavenumber spectra are measured with Doppler reflectometry in X-mode and O-mode wave polarizations at the same toroidal, poloidal and radial location. To our knowledge, this is the first time such a study has been conducted with Doppler reflectometry. Different spectral shapes were observed on Tore Supra in O- and X-mode at different locations, overlapping not being possible due to the strong magnetic field [62, 63]. The experimental wavenumber spectra are compared to

corresponding ones obtained via local nonlinear gyrokinetic simulation of the respective position in the plasma with the flux-code version of the GENE code [64]. The simulated density turbulence field is used as input to the 2D version of the finite difference time domain full-wave code IPF-FD3D [59], which has been adapted to the ASDEX Upgrade geometry [65]. The resulting wavenumber spectra are then compared to the experimental spectra.

This paper is organized as follows. Sections II and III introduce the experiment and the measured wavenumber spectra, respectively. These results are followed by the corresponding numerical simulations in Sec. IV, which are put into context in a discussion in Sec. V, followed by a short summary and conclusions in Sec. VI.

II. EXPERIMENTAL SETUP

In order to have the most reliable wavenumber spectra comparison from Doppler reflectometers measuring in X- and O-mode, three different reflectometer channels were connected to the same steerable Doppler antenna front-end [66]. The two channels used in X-mode configuration with frequencies in the W-band ($f = 75 - 110$ GHz) have a different backend [41, 67]; the V-band channel (($f = 50 - 75$ GHz) installed in O-mode has a scheme similar to one of the W-bands [67]. Since the cutoff-density of X-mode polarization is lower due to the magnetic field dependence of the X-mode cutoff, the different frequency ranges, in combination with the polarization configuration, enables the measurement of wavenumber spectra at the same toroidal, poloidal and radial position, but with X- and O-mode configuration.

Since different frequencies are employed, the beam sizes at the cutoff layer are different between O-mode and X-mode probing. In particular, the beam sizes ($1/e$ radius of electric field amplitude) are 2.8 cm and 1.9 cm for O-mode and X-mode, respectively. The radius of curvature of the cutoff layer at the measurement position is 62 cm, which results in spectral resolutions of $\Delta k_\perp = 2.1$ cm^{-1} (O-mode) and $\Delta k_\perp = 2.3$ cm^{-1} (X-mode). These estimates have been obtained following Ref. [68]. The spectral resolutions are not substantially different, such that the wavenumber spectra obtained in the following can be compared without further complications. In the full-wave simulations in Sec. IV B, the above beam sizes (and thus spectral resolutions) are included.

The discharges analyzed in this work have been obtained in upper single null (USN) configuration. Auxiliary heating has been provided by both neutral beam injection (NBI, 1 MW) and

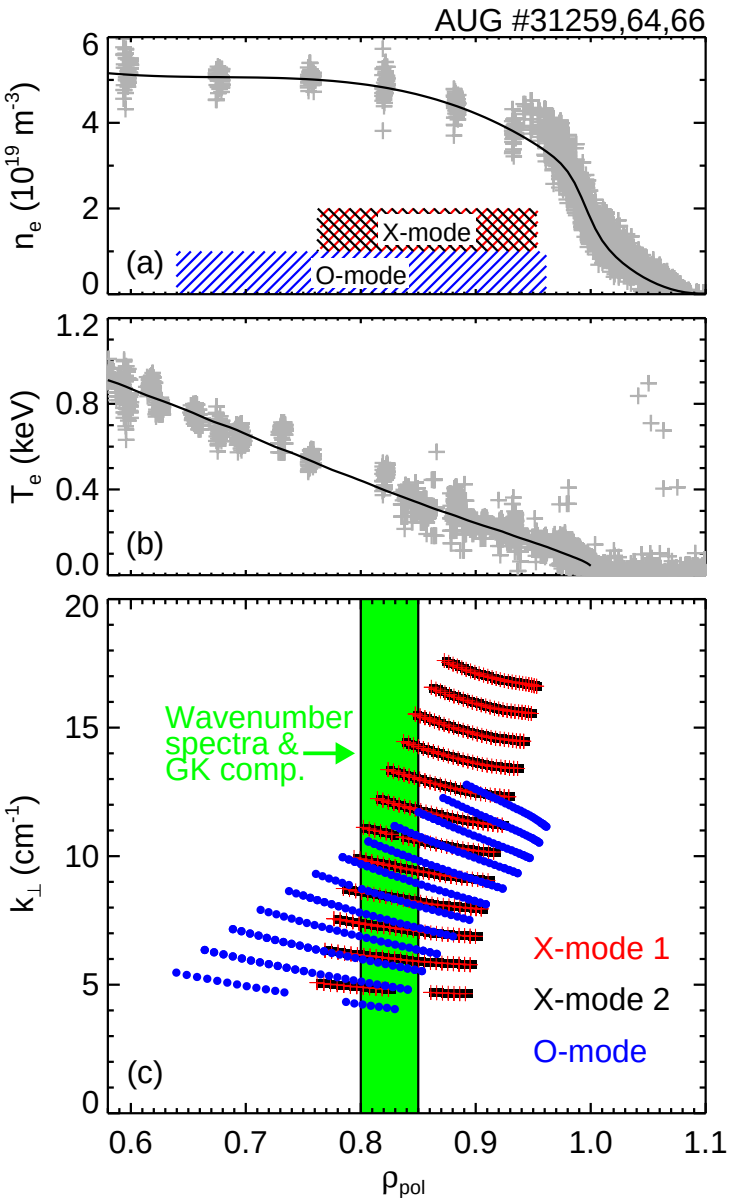

FIG. 1: Radial profiles of (a) electron density and (b) electron temperature. Measurements are shown in grey and fits are drawn as solid lines. (c) Perpendicular wavenumber space covered by Doppler reflectometry measurements in O-mode and X-mode. For details refer to the text.

electron cyclotron resonance heating (ECRH, 0.45 MW). With USN configuration, these plasmas usually stay in L-mode, since the input power is below both I-mode and H-mode power thresholds [69, 70].

Fig. 1(a) shows the electron density profile. Grey points indicate measurements obtained via the Thomson scattering (TS) [71] and lithium beam [72] diagnostics. The solid line shows the fit to the data, which is also used as input density profile for the TORBEAM beam-tracing code [73]

and the gyrokinetic simulations presented in Sec. IV A. For the fit, a modified tanh was used, and the resulting radial uncertainty is $\Delta\rho_{\mathrm{pol}} < 0.01$. The electron temperature profile is depicted in Fig. 1(b). Measurements are shown in grey and were obtained with TS and electron cyclotron emission (ECE) [74] systems. The fit (solid line) is a polynomial of third degree.

The perpendicular wavenumbers of turbulence $k_\perp$ probed by the Doppler reflectometer are plotted in Fig. 1(c). They are obtained using Torbeam, their uncertainties due to the density profile uncertainties are smaller than 0.2 cm^{-1}. The radial extent is mostly due to the frequency sweeps in the reflectometers while the $k_\perp$ variation is achieved by scanning the angle of incidence of the probing beam, which is done through a steerable mirror. Both X-mode (red, black) and O-mode (blue) measurements are indicated. To get a radial overlap of measurements, the frequencies used were 94.9 – 99.8 GHz (X-mode) and 62.0 – 66.8 GHz (O-mode). It can be observed that although the X-mode frequency span is comparable to the one of the O-mode, the radial extent of the measurement points is smaller, which is due to the magnetic field dependence of the X-mode cutoff. Furthermore, the O-mode covers a smaller wavenumber space, which is explained by the fact that $k_\perp$ probed by Doppler reflectometry depends on the vacuum wavenumber of the probing beam $k_\perp \propto k_0$, which is lower for the O-mode measurements due to the lower frequencies employed. The best combination of overlap in radius and $k_\perp$-space is obtained in the radial region of $\rho_{\mathrm{pol}} = 0.80 - 0.85$, which will be used for further analysis of wavenumber spectra and numerial simulation in the remainder of this paper.

Figure 1(c) shows the spectral distribution of the Doppler reflectometer measurements. In order to compare to gyrokinetic simulation and to setup the 2DFW simulations, the position of measurements in the poloidal plane is important. In Fig. 2, the poloidal cross-section of AUG is shown. Closed and open flux surfaces are shown as solid and dashed grey lines, respectively. The distribution of measurements is depicted for both X-mode and O-mode measurements. Again, all points are the result of beam-tracing calculations with the Torbeam-code on the density profile presented in Fig. 1(a). Furthermore, the radial region determined in Fig. 1(c) is indicated in green. The fact that the measurements are located in the upper part, roughly 30 cm above the midplane, has to be considered when comparing results to numerical simulations, which are presented later.

Typical frequency spectra obtained in X-mode and O-mode probing beam polarization are depicted in Fig. 3(a) and (b), respectively. Both spectra are measured at the same radial position with comparable wavenumbers ($\rho_{\mathrm{pol}} = 0.848$, $k_\perp = 5.9\ \mathrm{cm}^{-1}$ (X-mode) and $\rho_{\mathrm{pol}} = 0.847$, $k_\perp = 5.6\ \mathrm{cm}^{-1}$ (O-mode)). In both cases, the Doppler shifted component is clearly visible and roughly four or-

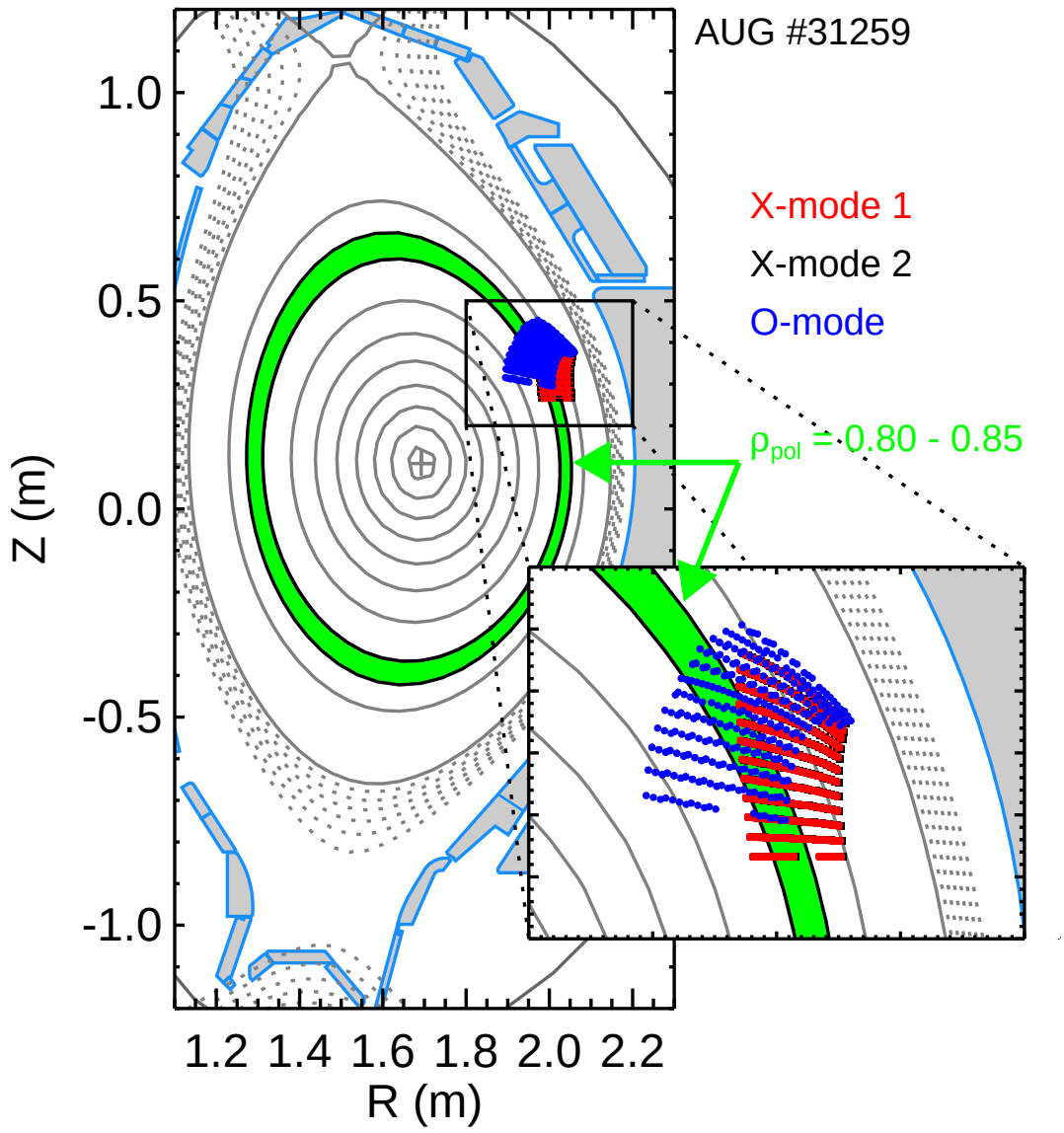

FIG. 2: Poloidal section of AUG. Closed flux surfaces are shown as solid grey lines, open flux surfaces are dashed. The Doppler reflectometer measurement positions are indicated in black and red for X-mode and blue for O-mode measurements. The radial range used for the estimation of wavenumber spectra is indicated in green. The inset shows a zoom to the measurement region.

ders of magnitude above the system noise level. Gaussian fits to the Doppler peaks (indicated in gray) are used to obtain the relevant information on Doppler shift f_D, Doppler peak width Δf_D and amplitude S_D. Since the turbulence level is proportional to the area under the Doppler peak, it is estimated as $\delta n^2 \propto S_D \Delta f_D$, which is used for the calculation of the wavenumber spectra presented in Sec. III. Since both X-mode and O-mode measure at the same position, the velocities

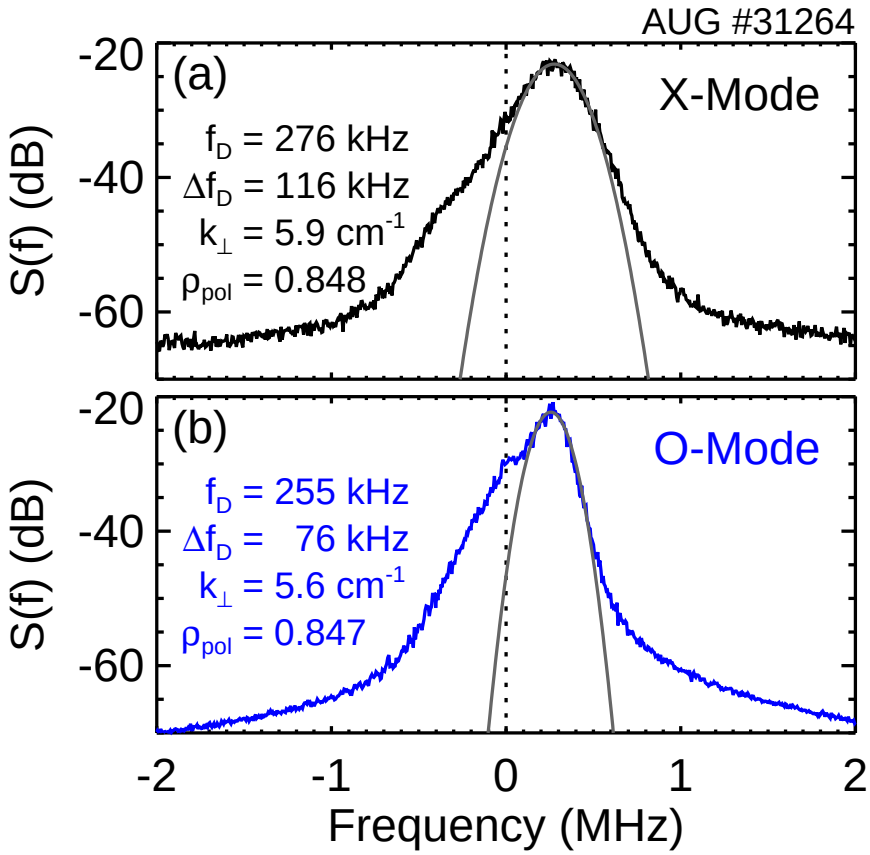

FIG. 3: Example frequency spectra for X-mode (a) and O-mode (b) polarization. Measurements are taken in the same plasma discharge at the same position with comparable wavenumber $k_\perp$. While the Doppler shift is comparable, a slightly wider Doppler shifted component is observed for the X-mode case.

$v_\perp = 2\pi f_D/k_\perp$ obtained should be comparable. Calculation yields $v_\perp = 2.94 \pm 0.10$ km/s (X-mode) and 2.87 ± 0.10 km/s (O-mode). An interesting observation is that although the spectral resolution is comparable, the X-mode Doppler peak is about 50% wider than the O-mode peak. This could be indicative of the X-mode probing in nonlinear regime and will be commented on in Sec. V.

III. WAVENUMBER SPECTRA

The wavenumber spectra obtained with the measurements presented above are shown in Fig. 4. The values are obtained by fitting a Gaussian to the asymmetric part of the power spectrum [75]. This gives the area under the Doppler shifted peak, which is proportional to the turbulence level. The probing beam frequencies used are 96.9 – 99.8 GHz (X-mode) and 62.0 – 66.8 GHz (O-mode). It should be pointed out that all spectra are from independent reflectometer electronics which

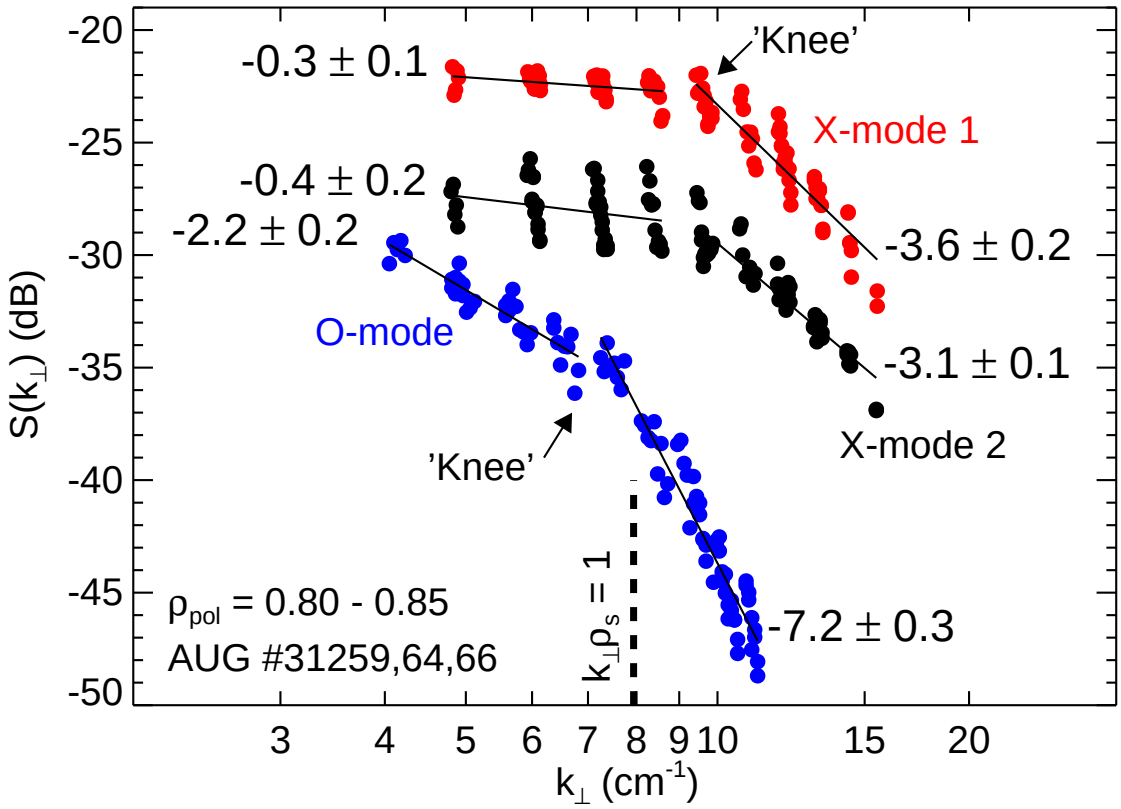

FIG. 4: Wavenumber spectra obtained for X-mode and O-mode polarizations with the same antenna system in the radial range $\rho_{\rm pol} = 0.80 - 0.85$, as indicated in Figs. 1 and 2. For comparison, the spectra have been offset vertically. Spectra obtained in X-mode and O-mode polarizations show pronounced differences.

share the same antennas for emission and reception. Since the Doppler channels do not deliver absolute density fluctuation levels, the spectra have been offset vertically in order to facilitate their comparison. The two spectra obtained in X-mode are shown in red and black, the one in O-mode is shown in blue. The first salient feature is the difference between the measured spectra, especially between O-mode and X-mode, although they still display a common behavior: the power spectral density falls off at a higher rate in the high $k_\perp$ range than at low $k_\perp$. Two power laws can roughly be fitted to the measurements on both sides of a 'knee', which appears at different positions for O-mode and X-mode. The X-mode spectra exhibit a flat region at low $k_\perp$ up to about $k_\perp = 9$ cm^{-1} with spectral indices of $\alpha = -0.3 \pm 0.1$ and -0.4 ± 0.2. At $k_\perp > 9$ cm^{-1}, a spectral fall-off is observed with spectral indices $\alpha = -3.6 \pm 0.2$ and -3.1 ± 0.1. Note that the uncertainties are the statistical uncertainties obtained via the fitting routine. Systematic uncertainties, which arise

by the ad hoc choice of the 'knee' position and the density profile used for the ray tracing, are not taken into account here. Hence, although strictly speaking the spectral indices at high $k_\perp$ are different when considering their statistical uncertainties, it is assumed that the two X-mode spectra are identical and the differences are caused by systematic but small uncertainties. It has to be noted that some measurements at low $k_\perp$ for X-mode 1 have been obtained with a partly saturated data acquisition system, which can be observed by the flat upper boundary of the measurements and the smaller data spread. This spread comes from the fact that with slightly higher probing frequency, the reflectometer measures slighlty further inside the plasma, where the turbulence level is lower. Since measurements here are taken from a radial range of $\rho_{\mathrm{pol}} = 0.80 - 0.85$, this effect is indeed visible. Nevertheless, the acquisition saturation is minimal and should not affect the wavenumber spectrum measurement by more than 2 dB. It should be stressed again that two different reflectometer back-ends have been used, one designed by IPP [41] and one by LPP [67]. The fact that the spectral shape is similar gives confidence in the reliability and reproducibility of the measurement.

In O-mode, two different spectral indices are observed, which are separated at a wavenumber of $k_\perp \approx 8\ \mathrm{cm}^{-1}$. Interestingly, the region at low $k_\perp$ is not flat as for the X-mode measurements, but it exhibits a spectral index of $\alpha = -2.2 \pm 0.2$. The spectral index in the high-$k_\perp$ region ($k_\perp > 8\ \mathrm{cm}^{-1}$) is with $\alpha = -7.2 \pm 0.3$ significantly more pronounced than in the X-mode spectra.

The flat region at low $k_\perp$ in the X-mode measurements seems to result from a saturation of the scattering response in X-mode, supported by the fact that the O-mode spectrum shows a finite spectral index of $\alpha = -2.2$ in the same low $k_\perp$ range. Nonlinear processes are indeed expected to appear for lower turbulence levels when probing fluctuations with X-mode polarization [54, 76]. This should also result in a shift of the knee position to higher $k_\perp$. More details and quantitative statements can be found in Sec. V.

The knee position, separating the regions of different spectral index, appears indeed at lower $k_\perp$ for the O-mode than for the X-mode, that is, slightly lower than $k_\perp \rho_s = 1$ for the O-mode, larger for the X-mode spectra. This spectral fall-off around $k_\perp \rho_s = 1$ has been observed previously in infrared laser scattering measurements [36], with spectral indices going from -3 at low k to -6 and more at higher k. In these experiments, the scattering efficiency is not expected to be affected by refraction processes during the wave propagation. This knee could suggest that while the linear growth rates might peak at larger scales, the fully developed turbulence could obtain its energy from the gradients through vorticity dynamics, which results in energy input close to

$k_\perp \rho_s = 1$ [77]. This is the case when the turbulent structures themselves extract energy from density and temperature profiles. Another possible explanation could be a transition from one regime of spectral energy transfer, incorporating critical balance between parallel and perpendicular characteristic times at scales $k_\perp \rho_i < 1$ [21] or energy transfer into damped eigenmodes [22], to another regime dominated by nonlinear phase mixing at $k_\perp \rho_i > 1$ [20]. Here, ρ_i is the characteristic ion gyroradius. However, instead of the piecewise power law, the data could be fitted by continuous functions, such as exponential [36, 78] or modified power law $k^{-3}/(1 + k^2)^2$ [23]. Indeed in tokamak plasmas, the turbulence drive is not expected to be well localized in k-space because of the rich spectrum of instabilities. Wavenumber spectra can significantly depart from usual power laws observed in fluid dynamics, when taking into account the interaction between large scale zonal flows and small scale turbulence [79].

In the measurements presented in this paper, the higher spectral index at $k_\perp > 8$ cm^{-1} for the O-mode spectra than for the X-mode spectra might also be due to the O-mode measuring in the linear regime while X-mode is measuring in the nonlinear or possibly the saturation regime [54, 55]. The interpretation of the above results in terms of linear and nonlinear probing regimes is supported by the fact that the corresponding 2D full-wave simulation results show the same trend, cf Sec. IV B. A detailed discussion and evaluation of the so-called nonlinearity parameter γ [54] is given in the discussion (cf Sec. V).

IV. NUMERICAL RESULTS

Since both X- and O-mode spectra were measured on the same plasma at the same position, it is highly probable that the pronounced difference of experimental wavenumber spectra in the two probing beam polarizations is a diagnostic effect. In order to prove this statement, turbulence has been generated by gyrokinetic simulation [80], which is nowadays the most advanced tool for describing core plasma microturbulence. The resulting turbulence field then serves as input for two-dimensional full-wave simulation, which includes all relevant wave physics for the description of the backscattering process used in Doppler reflectometry measurements. As in the experiment, the 2D full-wave simulations are performed in O- and X-mode polarization and then compared to the experimental findings.

A. Wavenumber spectra from gyrokinetic simulation

The theoretical description nowadays considered most appropriate for assessing core plasma microturbulence is the so-called gyrokinetic theory [80]. Over the last decades, a number of numerical implementations of the underlying set of equations has been developed [64, 81–86]. Here, the tool chosen for the further evaluation is the gyrokinetic code GENE [64] that can be used either in (local) flux-tube geometry, as a full torus code or considering a flux surface. As the latter two operational modes can be quite expensive in terms of computational time, flux-tube simulations local to the flux surface around $\rho_{\mathrm{tor}} = 0.75$ have been performed to characterize the underlying microinstabilities and produce turbulence fields for further processing with the full wave code and direct comparison with the experimental measurements. Here, $\rho_{\mathrm{tor}} = \sqrt{\Psi_{\mathrm{tor}}/\Psi_{\mathrm{tor,sep}}}$ denotes the normalized toroidal flux surface label with the toroidal flux Ψ_{tor} and its separatrix value $\Psi_{\mathrm{tor,sep}}$.

The simulation physics input parameters evaluated from the ASDEX Upgrade discharge #31260 at $t = 3\,\mathrm{s}$ and this radial position can be summarized as follows. The reference values are given by the magnetic field on axis $B_{\mathrm{ref}} = 2.5\,\mathrm{T}$, the electron temperature $T_{\mathrm{ref}} = T_e = 319\,\mathrm{eV}$, the electron density $n_{\mathrm{ref}} = n_e = 4.62 \cdot 10^{19}\,\mathrm{m}^{-3}$, the unnormalized ρ_{tor} value at the separatrix $L_{\mathrm{ref}} = a = 0.646\,\mathrm{m}$, the deuterium mass $m_{\mathrm{ref}} = m_D$ and the background toroidal angular velocity $\Omega_{\mathrm{tor,ref}} = 6 \cdot 10^4\,\mathrm{rad/s}$. This choice determines the reference velocity $v_{\mathrm{ref}} = c_s = 123.92\,\mathrm{km/s}$ and the gyroradius normalization, $\rho_{\mathrm{ref}} = \rho_s = 1.03\,\mathrm{mm}$, and hence the finite-size parameter $\rho^* = \rho_s/L_{\mathrm{ref}} = 1/628$. With the latter being very small, further confidence in the validity of the local approach for the scenario at hand is gained. The reference values are furthermore used to consistently determine the parameters associated with co-moving-frame effects, collisions (modeled via a linearized Landau-Boltzmann collision operator) and (perpendicular) electromagnetic fluctuations which are all considered in the GENE simulations. Furthermore, (external) $E \times B$ flow shearing and parallel flow shear effects are included in the nonlinear simulations. The relevant input is here $\gamma_E = -\frac{\rho}{q_0}\frac{\partial \Omega_{\mathrm{tor}}}{\partial \rho}\frac{a}{c_s} = 4.64 \cdot 10^{-2}$. For now, only deuterium as the main ion species and electrons are explicitly considered in the simulations while impurities are only taken into account through the $Z_{\mathrm{eff}} = 1.5$ factor in the collision operator. Due to the quasi-neutrality condition, n_i is assumed to be equal to n_e and consistently both logarithmic density gradients are given by $a/L_n = -\partial/\partial\rho \ln n_e = 0.94$. Due to a lack of ion temperature measurements, a similar assumption for T_i is the most reasonable choice for this situation. Therefore, $T_i = T_e$ and

$a/L_{Ti} = a/L_{Te} = -\partial/\partial\rho \ln T_e = 4.60$. Finally, the metric coefficients are directly extracted from the equilibrium code CLISTE [87] via a field line tracing algorithm [88]. The flux surface of interest is characterized by a safety factor of $q_0 = 2.19$ and a magnetic shear of $\hat{s} = \frac{\rho}{q_0}\frac{\partial q}{\partial \rho} = 1.61$.

The numerical grids have been chosen as follows. In velocity space, 48 and 16 grid points have been considered in the $v_\parallel$ velocity along the magnetic field direction and for the magnetic moment μ. The associated boxes are given by $-3\, v_{th,j}$ to $3v_{th,j}$ in the first and 0 to $9T_{0j}/B_{\mathrm{ref}}$ for the second direction. Here, $v_{th,j} = \sqrt{2T_{0j}/m_j}$ denotes the thermal velocity of the j-th species ($j = i, e$) with mass m_j and temperature T_{0j}. In configuration space, 24 grid points for one poloidal turn are considered in the (z) direction parallel to the magnetic field line. Based on convergence tests, $(512, 192)$ grid points and a size of $(L_x, L_y) = (182.5, 123)\rho_s$ have been found sufficient along the remaining radial (x) and binormal (y) directions for the nonlinear simulations. Less grid points can be used in linear simulations since the box sizes can be adjusted to the individual modes here. Such linear runs are typically performed to identify the main microinstabilities at play. In the given context, parameter scans within the error bars of the temperature and density gradients and the Z_{eff} value showed robust ion temperature gradient (ITG) driven modes in the low-k (ion-gyroradius scale) range while trapped electron (TEM) and electron temperature gradient (ETG) driven modes become dominant in the sub-ion-gyroradius scale regime. One such spectrum of the linear growth rates and the real frequencies can be found in Fig. 5(a-c). ITG modes propagate in ion-diamagnetic direction (positive frequencies) and ETG modes propagate in electron-diamagnetic direction (negative frequencies). Note the different frequency axis ranges in Fig. 5(b-c). The density gradient and Z_{eff} are only weakly affecting the linear growth rates and frequencies while a/L_T is found to introduce quantitative changes – qualitatively the modes stay unchanged.

Initial nonlinear simulations with the nominal gradients yield a total heat flux about two times larger than the expected value from the experiment of $P_{\mathrm{tot}}^{\mathrm{exp}} \approx 2.1\,\mathrm{MW}$. With the linear findings in mind, a scan along a/L_T has hence been performed in order to achieve flux matching. The best results have been achieved with a 20% reduction ($a/L_T = 3.68$) where the heat flux from GENE evaluates to $P_{\mathrm{tot}}^{\mathrm{GENE}} \approx 2.15 \pm 0.50\,\mathrm{MW}$. It should be noted that these simulations did not include the ETG range but had to be cut around $k_y\rho_s \approx 4.85$. An artificial spectral pile-up at this wave number due to finite turbulence drive at these scales is avoided by gyro-LES methods [89]. The corresponding density spectrum at zero radial wavenumber and $(R, Z) = (2.019, 0.321)\,\mathrm{m}$ (cf Fig. 2) which is a lowest-order approximation of a synthetic Doppler reflectometry can be found in Fig. 5(d) with a zoom to the part relevant for the experiment comparison depicted in

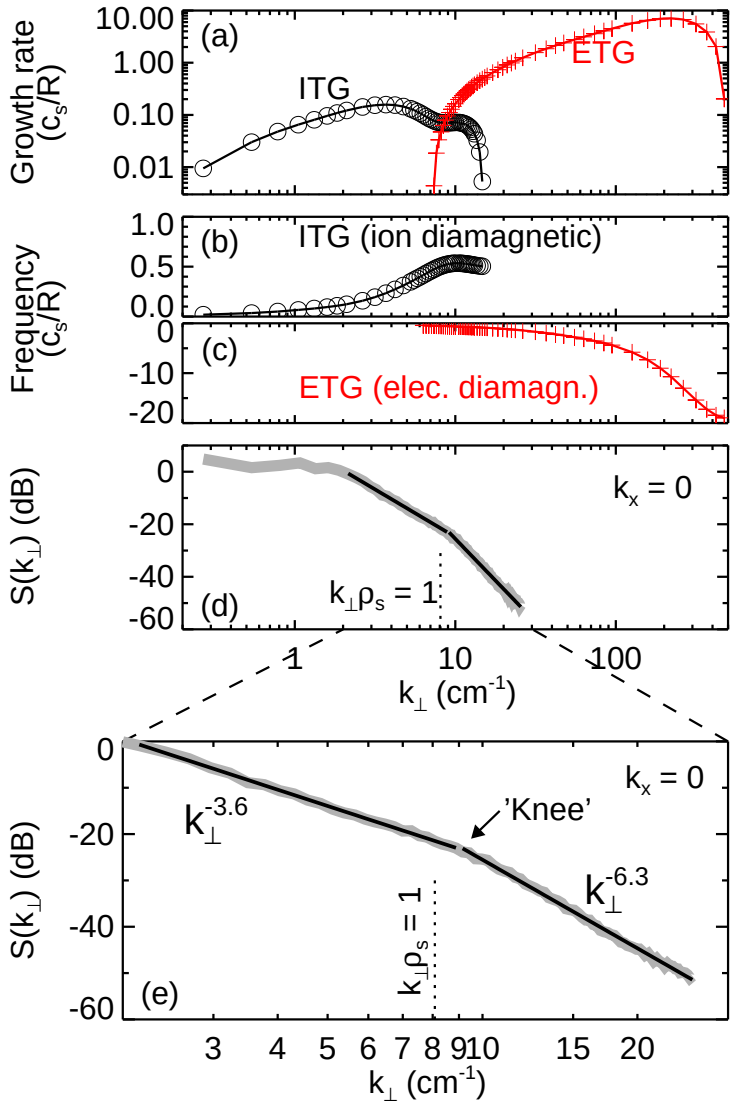

FIG. 5: Results from gyrokinetic simulation. (a) Linear growth rate of fastest growing mode, (b,c) corresponding real mode frequencies (note the different y-axis ranges), (d) density wavenumber spectrum from nonlinear simulation, (e) zoom to experimentally relevant range. The density wavenumber spectrum exhibits two distinct power laws with a transition point ('knee') at $k_\perp \approx 9$ cm^{-1}.

Fig. 5(e). The turbulence level (integrated over all radial wavenumbers k_x) resulting from this simulation is $\delta n_{\mathrm{RMS}}/n_0 = 2.1\%$ for the full flux surface and $\delta n_{\mathrm{RMS}}/n_0 = 2.7\%$ at the corresponding measurement location. The higher value at the measurement location (on the low-field side) is due to the ballooning character of the turbulence. At the measurement location and only taking into account small k_x, $\delta n_{\mathrm{RMS}}/n_0 = 0.9\%$. This value has been obtained by integrating the wavenumber spectrum around $k_x = 0$ with limits $[-k_{x,\mathrm{min}}/2,\ k_{x,\mathrm{min}}/2]$, where $k_{x,\mathrm{min}} = 2\pi/L_x \approx 0.33$ cm^{-1}.

Since the Doppler reflectometer beam has a non-negligible radial size, it will measure the $k_\perp$-spectrum around $k_r = 0$ [8, 16, 48, 51]. The closest approximation to that without using a synthetic diagnostic or advanced filtering is the $k_\perp$ spectrum at $k_x = 0$, which is plotted in Fig. 5 (d-e).

As in the experiment, two distinct power laws are found with a spectral break that closely resembles the 'knee' point of the O-mode measurement. Investigation into the nature of this knee is ongoing at the moment. As mentioned in Sec. III, it could be a transition from one regime of spectral energy transfer, incorporating critical balance between parallel and perpendicular characteristic times at scales $k_\perp \rho_i < 1$ [21] or energy transfer into damped eigenmodes [22], to another regime dominated by nonlinear phase mixing at $k_\perp \rho_i > 1$ [20]. Although the values of the spectral indices do not agree with the ones derived in the above references, the physics could still play a role and manifest itself in the spectral shape. The spectral indices in Fig. 5(e) are in good qualitative agreement with the experiment, i.e. the one at higher wavenumbers is about twice as large as the one at low wavenumbers. Quantitatively, some disagreement is left. The power law from gyrokinetic simulation is slightly steeper at low-$k_\perp$ (-2.2 / -3.6) and more shallow at high-k (-7.2, -6.3) compared to the measurements. In order to assess a possible impact of nonlinearities and saturation on these results, the simulated density fluctuations, which are considered as the "real" spectrum, have been mapped on a torus and translated to the lab frame. They are used as input for further analysis with a full wave code, which produces a synthetic spectrum to be compared with the experiment, as will be detailed in the next section.

B. Two-dimensional full-wave simulation results

The turbulence field obtained via gyrokinetic simulations in Sec. IV A serves as input to the two-dimensional version of the three-dimensional full-wave code IPF-FD3D [59, 65]. As before, to do a meaningful comparison, the same region of the poloidal cross-section as in the experiment has to be probed by the full-wave code.

The simulation domain is $R = [1.800\,\text{m}, 2.265\,\text{m}]$, $Z = [0.120\,\text{m}, 0.640\,\text{m}]$, covering the region where the wave propagates. At the $R = 2.265$ m boundary, virtual transmitter and receiver antennas were placed, according to the antenna patterns at that location. IPF-FD3D is a finite difference time domain (FDTD) code that solves the Maxwell curl equations and the cold plasma electron current on a cartesian grid with fixed time step $\Delta t = 0.5\Delta x/c$ using a Crank-Nicolson scheme. The maximum frequencies injected into the grid were 103 GHz for X-mode and 75 GHz for O-mode

with spatial steps $\Delta x_X = 0.2221$ mm and $\Delta x_O = 0.1617$ mm, respectively.

Beams for all angles between $-7°$ and $7°$ with half-degree stepping are injected simultaneously. Their frequencies have been chosen using TORBEAM for a turning point at $\rho_{pol} = 0.825$, according to the central point of the radial window from the experimental observation. Because of the different frequencies, the relative cross talk between different beams at the receiver is less than 10^{-7}. Therefore, in one simulation run, all wavenumbers are probed simultaneously against a fixed background of density fluctuations (turbulence snapshot). The simulation is then repeated for each available density fluctuation field. All 512 turbulence snapshots were used in the simulation, yielding a received amplitude and phase for each beam and each snapshot. The spectral power for each beam was estimated using the variance of the amplitude for each beam.

Figure 6 shows the spatial setup of the two-dimensional full-wave simulation with O-mode wave polarization. The density turbulence field calculated from gyrokinetic simulation is color-coded, while the contours of the wave electric field E are overlayed. Most scattering of the wave takes place in a region corresponding to the experimental situation (cf Fig. 2). Furthermore, the whole study is repeated for the X-mode case in order to have the best possible comparison to the experimental results detailed in Sec. II.

The wavenumber spectra resulting from the full-wave simulations in both O- and X-mode polarization are depicted in Fig. 7. While the backscattered power is comparable between X-mode and O-mode at low $k_\perp \approx 3 - 4$ cm^{-1}, the wavenumber spectra differ substantially at $k_\perp > 4$ cm^{-1}. The X-mode spectrum is comparably flat ($\alpha = -0.6 \pm 0.1$) up to a value of $k_\perp \approx 11$ cm^{-1}, where a weak spectral fall-off with a spectral index of $\alpha = -2.3 \pm 0.2$ starts. In contrast, the O-mode spectrum shows a spectral fall-off at low $k_\perp$ ($\alpha = -1.5 \pm 0.1$), and exhibits a pronounced fall-off with a spectral index of $\alpha = -8.8 \pm 0.1$ at $k_\perp > 6$ cm^{-1}. Hence, the scales where the spectral fall-off starts (marked 'Knee' in Fig. 7) are larger than $k_\perp \rho_s = 1$ for O-mode and smaller than $k_\perp \rho_s = 1$ for X-mode. The spectral 'knee', observed in gyrokinetic simulation at $k_\perp \approx 9\,\mathrm{cm}^{-1}$ (cf Fig. 5(d)), is recovered in 2D full-wave simulation, but at smaller $k_\perp$ for O-mode and larger $k_\perp$ for X-mode. While the knee position at larger $k_\perp$ in the X-mode case could possibly be explained by a saturation of the measurements at low $k_\perp$, it is unclear why the knee is observed at lower $k_\perp$ for the O-mode case. The origin of this difference between the wavenumber spectrum from gyrokinetic simulation and the one obtained via full-wave analysis is investigated at the moment.

It is obvious that neither the wavenumber spectrum measured with O-mode nor the one measured with X-mode wave polarization reproduces directly the wavenumber spectrum of the in-

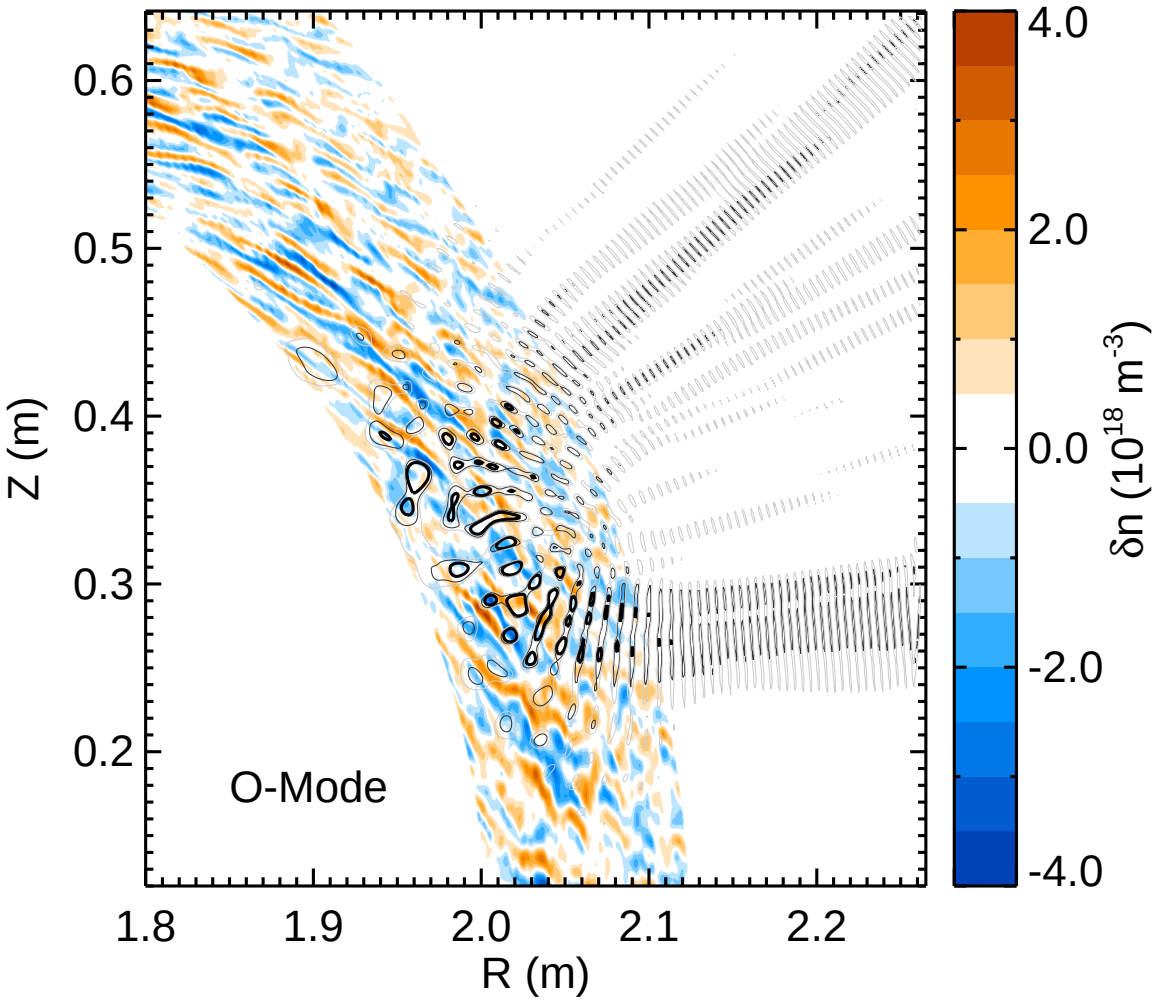

FIG. 6: 2D full wave simulation setup for O-mode. The turbulence field calculated by the gyrokinetic code is color-coded while contours of the wave electric field E are overlayed. Darker contours correspond to stronger E_R. Close to the probing beam turning point, the maximum in the wave electric field is observed and backscattering takes place.

put (cf Fig. 5). The synthetic X-mode spectrum underestimates the spectral fall-off substantially, which is at least in part due to an overestimation of power related to the so-called regimes of nonlinear and saturated probing [55, 76, 90]. Multiplication of the turbulence field by 0.5 and repetition of the simulation run (pink circles) results in slightly less power at high $k_\perp$, while low $k_\perp$ are not affected because they are deeply in the saturated regime. While the spectrum measured in O-mode polarization is not in perfect agreement with the input spectrum either, it gives at least results which are closer to the input spectrum than the spectrum measured in X-mode. For the O-mode spectrum, the spectral fall-off at low $k_\perp$ is underestimated while it is overestimated at high

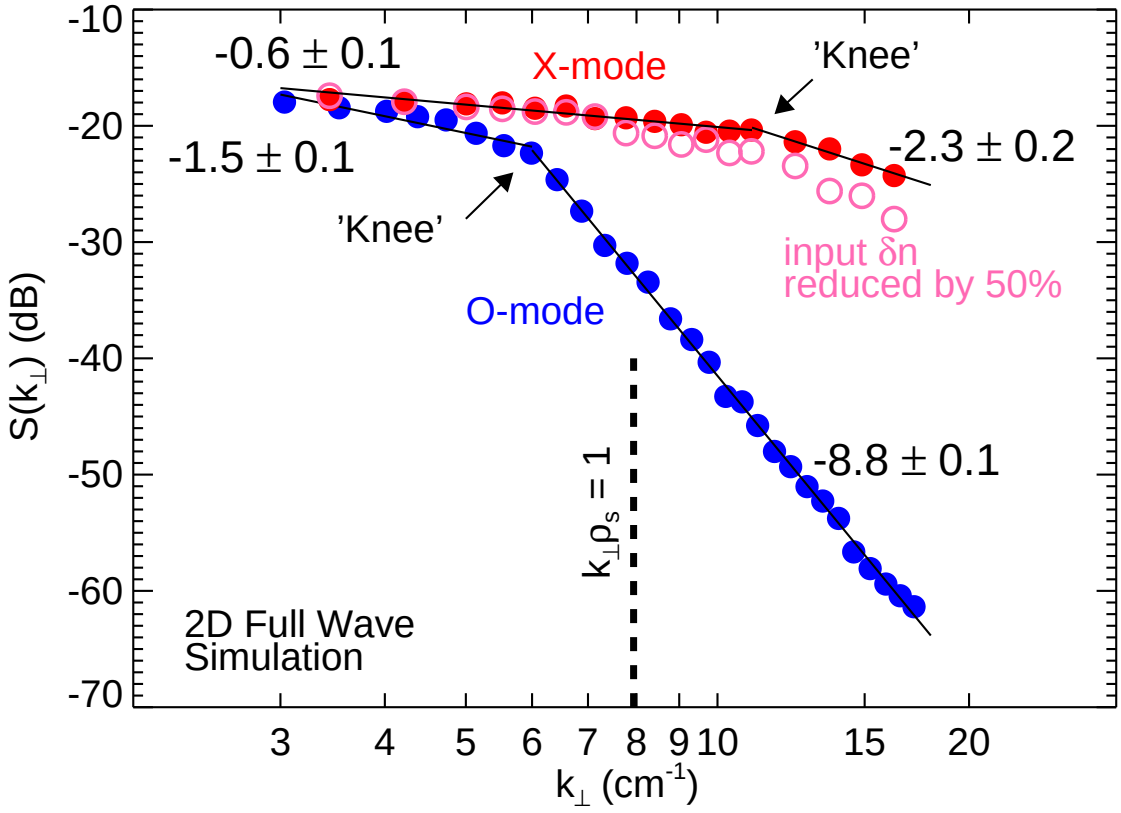

FIG. 7: Wavenumber spectra obtained from 2DFW simulation applied to the turbulence field calculated by gyrokinetic simulation. Both O-mode (blue) and X-mode (red) results are shown.

$k_\perp$.

Recalling the experimental results (cf Fig. 4), the synthetic diagnostic reproduces a variety of effects. It is important to point out again that in both experiment and simulation, the wavenumber spectrum measurement is at the same location, and measurements take place simultaneously, i.e. the density turbulence probed with O- and X-mode is the same. Several aspects observed experimentally are reproduced in the full-wave simulation: first, the spectral 'knee' is at larger scales for O-mode than for X-mode. Second, a flat part is seen in the X-mode spectrum up to a value of $k_\perp \approx 12$ cm^{-1}, where the steep spectral fall-off starts. Third, the spectral indices in both low-$k_\perp$ and high-$k_\perp$ regions are more pronounced in O-mode than in X-mode. These points convincingly show that the wavenumber spectra measured in the experiment in X- and O-mode are different due to a diagnostic effect, which is intrinsic to Doppler reflectometry, hence directly reproduced in 2D full-wave simulations.

V. DISCUSSION

The reliable measurement of wavenumber spectra is of highest importance not only for experimental turbulence investigations, but also for the validation of gyrokinetic codes. However, the results of this paper show that care must be taken when interpreting experimental wavenumber spectra obtained by Doppler reflectometry. The experimental observation of a pronounced difference between wavenumber spectra measured in O- or X-mode polarization from the same antenna at the same toroidal, poloidal, and radial location questions at least the validity of wavenumber spectra measured via Doppler reflectometry in nonlinear probing regimes, which is more likely the case for X-mode probing wave polarization. The measurements presented in this paper have been obtained in the core plasma at $\rho_{\mathrm{pol}} = 0.80 - 0.85$. Taking into account that core turbulence levels are expected to be significantly lower than edge turbulence levels, the results of this paper should also be valid for edge Doppler reflectometry measurements.

Using a comprehensive suite of tools for the validation of gyrokinetic codes is important. This is true in particular in cases when diagnostics are subject to non-trivial effects such as plasma-wave interactions, nonlinearities or saturation. In these cases, it is mandatory to use synthetic diagnostics which can model to sufficient degree the complexities of the measurement. In the optimum case, the synthetic diagnostic is able to capture all physics effects with impact on the measurement. Due to computational time, it is counterproductive to incorporate more into the simulation than needed. In this paper, this situation has been detailed by presenting experimental wavenumber spectra with pronounced differences due to the probing beam polarization. These differences have been reproduced using turbulence from a gyrokinetic code as input for two-dimensional full-wave simulation.

An evaluation of whether measurements were taken in linear or nonlinear regimes can be obtained via the so-called nonlinearity parameter [54]

$$\gamma = \left(\frac{\delta n}{n}\right)^2 \frac{G^2 \omega^2 x_c l_{cx}}{c^2} \ln \frac{x_c}{l_{cx}}. \tag{1}$$

Measurements are taken in the linear regime for $\gamma \ll 1$ or in the nonlinear regime for $\gamma > 1$. Here, $\delta n/n$ is the turbulence level, $\omega = 2\pi f$ is the probing wave frequency, x_c is the distance from plasma periphery to the cutoff layer, l_{cx} is the radial correlation length, and c is the speed of light in vacuum. The quantity G is the polarization-dependent enhancement factor and can be found in Ref. [91]. Values used for the evaluation of (1) are $\delta n/n = 0.9\%$ and $l_{cx} = 0.031$ m (both from gyrokinetic simulation, see Sec. IV A), $x_c = 0.25$ m, $f_{\mathrm{O}} = 64.4$ GHz (O-mode), $f_{\mathrm{X}} = 97.4$ GHz

(X-mode), $G_O = 1$ and $G_X = 3.9$. Resulting values are $\gamma_O = 2.4$ (O-mode) and $\gamma_X = 81.6$ (X-mode). This is a pronounced difference of more than one order of magnitude and it shows that the measurements have been obtained close to the transition from linear to nonlinear regime in the O-mode while X-mode is more likely to be in the nonlinear or even saturation regime. Hence, it is a parameter regime where strong differences between O-mode and X-mode are to be expected. An extension to the above formula to include Doppler reflectometry has been proposed [55] which yields a comparable result, with $\gamma_X \approx 10\gamma_O$.

A more direct indication that the X-mode system is measuring in the nonlinear regime is provided by the fact that the Doppler shifted component in the X-mode spectrum is wider than the one obtained with O-mode probing beam polarization. This can be seen in Fig. 3, where the X-mode Doppler peak is about 50% wider than the O-mode peak, although both systems measure at the same radial position and the spectral resolutions of both systems are comparable. This broadening of the Doppler peak in the nonlinear regime has been predicted theoretically and is strongest for sheared velocity profiles [92]. For the case at hand, the velocity profile is not strongly sheared ($\mathrm{d}v_\perp/\mathrm{d}R \approx 22 \cdot 10^3\ \mathrm{s}^{-1}$). Hence, it should be noted that although existent, the difference in spectrum width is not very pronounced and should be regarded as indicative. The parameter γ and the flatness of the X-mode spectrum at low $k_\perp$ are clearer signs for the nonlinearity of the measurements.

It is interesting to estimate the required turbulence level $\delta n/n$, for which (1) would yield a transition to linear regime for the X-mode measurements. The assumption is made that, apart from the turbulence level, quantities like density profile and magnetic field are fixed, which results in G, ω and x_c unchanged with respect to the considerations above. Also l_{cx} is assumed to be fixed. For the X-mode to measure close to the linear regime, i.e. $\gamma_X = 1$, a turbulence level of $\delta n/n = 0.1\%$ would be necessary, which is a factor 9 lower than the one predicted by the gyrokinetic simulations in Sec. IV A. In principle, one can imagine such low turbulence levels in the core region or in H-mode edge plasmas. It should be emphasized that an estimation of (1) to determine the reliability of wavenumber spectra measurements is strongly recommended.

However, this does not mean that turbulence level measurements with Doppler reflectometry in the nonlinear regime are futile. Important effects such as relative changes can be measured even if a Doppler reflectometer measurement is done at $\gamma > 1$. While quantitative statements might be difficult to make, at least qualitative conclusions, such as a reduction of turbulence level at a specific wavenumber or a qualitative comparison of turbulence levels at different wavenumbers, is

possible. This is exemplified with the X-mode spectra of Fig. 4 at $k_\perp > 9$ cm^{-1}: the decay with $k_\perp$ indicates that the measurements are not saturated (assuming the *real* wavenumber spectrum decays with $k_\perp$, which is a reasonable assumption). Although not saturated, these measurements could still originate from the nonlinear regime, which can result in shallower spectral indices compared to the input wavenumber spectrum [55]. In the extreme case of saturation ($\gamma \gg 1$, treated in Ref. [92]), other effects such as spectrum broadening due to multiple forward scattering or wave trapping can even lead to an inverse response of the Doppler reflectometer [55], and even qualitative statements cannot be made anymore. This could be the case for the X-mode spectra in Fig. 3 at $k_\perp < 9$ cm^{-1}. These parts of the spectra should be regarded with particular care due to their flatness, which seems to indicate that they are saturated.

It should be pointed out that these results apply to backscattering experiments in which the refractive index approaches zero close to the cutoff layer, where strong plasma-wave interactions take place. These effects are nonexistent in scattering experiments with refractive indices close to unity, as e.g. in far-infrared laser scattering experiments [36]. These diagnostics should not be affected by the issues detailed in this paper.

VI. SUMMARY AND CONCLUSIONS

The process for meaningful wavenumber spectrum analysis, which can contribute to the validation of gyrokinetic codes, has been detailed from measurement, through gyrokinetic simulation, and the application of a synthetic diagnostic. These ingredients are required in order to do meaningful validation studies. This paper details the intricacies when using wavenumber spectra for validation.

In detail, wavenumber spectra have been measured in the ASDEX Upgrade tokamak via Doppler reflectometry in X-mode and O-mode wave polarization. The main experimental findings are a pronounced difference between X- and O-mode spectra and the confirmation of the existence of a knee in the spectra at $k_\perp \rho_s \approx 1$.

Accompanying linear and nonlinear local gyrokinetic simulations with the GENE code have been performed. The ion-temperature-gradient mode is the fastest growing mode in the scenario, and the resulting density turbulence wavenumber spectrum is dominated by fluctuations at $k_\perp < 2$ cm^{-1}. Two regions in the wavenumber spectrum with different spectral energy transfer behavior have been observed. The boundary between these two regions is at $k_\perp \approx 9$ cm^{-1}. The reason for the

existence of these two clearly separated regions is investigated at the moment.

Two-dimensional full-wave simulations are in good qualitative agreement with the experimental measurements, reproducing the experimental observation that X-mode spectra tend to be comparably flat while spectra measured with O-mode wave polarization show a clear spectral fall-off. Estimation of the nonlinearity parameter γ shows that while the O-mode measurements have been done close to the transition from linear to nonlinear regime, the X-mode measurements have been made in the nonlinear or even saturation regime. When measurements are expected to be in the saturation regime, which can result in flat wavenumber spectra, such measurements should be treated with particular caution.

For experimental turbulence investigations and the validation of gyrokinetic codes in terms of wavenumber spectra, these findings show that Doppler reflectometry in O-mode wave polarization is better suited than in X-mode, which is because of the polarization-dependent enhancement factor G in the nonlinearity parameter (1). However, the better spatial localization makes X-mode better suited for perpendicular propagation velocity measurements. Therefore, the predominant use of a future Doppler reflectometer should be taken into account during its design phase. Diagnostics allowing for both O- and X-mode polarizations are preferable due to their optimum applicability to both wavenumber spectra and turbulence propagation velocity studies.

In terms of gyrokinetic code validation, the most important task of the experimentalist is to provide measurements of different quantities which give the maximum number of restraints on the gyrokinetic code output. These quantities are, apart from wavenumber spectra, density and electron temperature fluctuations and the cross-phases between them, radial and poloidal correlation lengths, and the tilt angle of turbulent structures. To advance these validation studies, a "turbulence comparison discharge" comprising the aforementioned measurements is planned for the next ASDEX Upgrade campaign and will be used as a gyrokinetic code validation discharge.

Acknowledgments

This work was partly performed in the framework of the Helmholtz Virtual Institute on plasma dynamical processes and turbulence using advanced microwave diagnostics (VH-VI-526) and within the framework of the EUROfusion Consortium and has received funding from the Euratom research and training programme 2014-2018 under grant agreement No 633053. The fullwave simulations were performed on bwUniCluster funded by the Ministry of Science, Research and

Arts and the Universities of the State of Baden-Württemberg, Germany, within the framework program bwHPC. The gyrokinetic simulations presented in this work were carried out using the HELIOS supercomputer system at Computational Simulation Centre of International Fusion Energy Research Centre (IFERC-CSC), Aomori, Japan, and at the Max Planck Computing and Data Facility (MPCDF), Garching, Germany. Furthermore, funding from the EUROfusion Enabling Research work-package AWP15-ENR-09/IPP-02 is acknowledged. The views and opinions expressed herein do not necessarily reflect those of the European Commission.

---

[1] A. M. Dimits, G. Bateman, M. A. Beer, B. I. Cohen, W. Dorland, G. W. Hammett, C. Kim, J. E. Kinsey, M. Kotschenreuther, A. H. Kritz, L. L. Lao, J. Mandrekas, W. M. Nevins, S. E. Parker, A. J. Redd, D. E. Shumaker, R. Sydora, and J. Weiland, Phys. Plasmas **7**, 969 (2000).

[2] W. M. Nevins, J. Candy, S. Cowley, T. Dannert, A. Dimits, W. Dorland, C. Estrada-Mila, G. W. Hammett, F. Jenko, M. J. Pueschel, and D. E. Shumaker, Phys. Plasmas **13**, 122306 (2006).

[3] W. M. Nevins, S. E. Parker, Y. Chen, J. Candy, A. Dimits, W. Dorland, G. W. Hammett, and F. Jenko, Phys. Plasmas **14**, 084501 (2007).

[4] M. J. Pueschel, M. Kammerer, and F. Jenko, Phys. Plasmas **15**, 102310 (2008).

[5] G. L. Falchetto, B. D. Scott, P. Angelino, A. Bottino, T. Dannert, V. Grandgirard, S. Janhunen, F. Jenko, S. Jolliet, A. Kendl, B. F. McMillan, V. Naulin, A. H. Nielsen, M. Ottaviani, A. G. Peeters, M. J. Pueschel, D. Reiser, T. T. Ribeiro, and M. Romanelli, Plasma Phys. Control. Fusion **50**, 124015 (2008).

[6] R. V. Bravenec, J. Candy, M. Barnes, and C. Holland, Phys. Plasmas **18**, 122505 (2011).

[7] A. E. White, L. Schmitz, G. R. McKee, C. Holland, W. A. Peebles, T. A. Carter, M. W. Shafer, M. E. Austin, K. H. Burrell, J. Candy, J. C. DeBoo, E. J. Doyle, M. A. Makowski, R. Prater, T. L. Rhodes, G. M. Staebler, G. R. Tynan, R. E. Waltz, and G. Wang, Phys. Plasmas **15**, 056116 (2008).

[8] A. Casati, T. Gerbaud, P. Hennequin, C. Bourdelle, J. Candy, F. Clairet, X. Garbet, V. Grandgirard, O. D. Gürcan, S. Heuraux, G. T. Hoang, C. Honoré, F. Imbeaux, R. Sabot, Y. Sarazin, L. Vermare, and R. E. Waltz, Phys. Rev. Lett. **102**, 165005 (2009).

[9] M. Greenwald, Phys. Plasmas **17**, 058101 (2010).

[10] C. Holland, L. Schmitz, T. L. Rhodes, W. A. Peebles, J. C. Hillesheim, G. Wang, L. Zeng, E. J. Doyle, S. P. Smith, R. Prater, K. H. Burrell, J. Candy, R. E. Waltz, J. E. Kinsey, G. M. Staebler, J. C. DeBoo,

C. C. Petty, G. R. McKee, Z. Yan, and A. E. White, Phys. Plasmas **18**, 056113 (2011).

[11] C. Holland, J. DeBoo, T. Rhodes, L. Schmitz, J. Hillesheim, G. Wang, A. White, M. Austin, E. Doyle, W. Peebles, C. Petty, L. Zeng, and J. Candy, Nucl. Fusion **52**, 063028 (2012).

[12] C. Holland, C. Petty, L. Schmitz, K. Burrell, G. McKee, T. Rhodes, and J. Candy, Nucl. Fusion **52**, 114007 (2012).

[13] S. Leerink, V. V. Bulanin, A. D. Gurchenko, E. Z. Gusakov, J. A. Heikkinen, S. J. Janhunen, S. I. Lashkul, A. B. Altukhov, L. A. Esipov, M. Y. Kantor, T. P. Kiviniemi, T. Korpilo, D. V. Kuprienko, and A. V. Petrov, Phys. Rev. Lett. **109**, 165001 (2012).

[14] A. E. White, N. T. Howard, M. Greenwald, M. L. Reinke, C. Sung, S. Baek, M. Barnes, J. Candy, A. Dominguez, D. Ernst, C. Gao, A. E. Hubbard, J. W. Hughes, Y. Lin, D. Mikkelsen, F. Parra, M. Porkolab, J. E. Rice, J. Walk, S. J. Wukitch, and the Alcator C-Mod Team, Phys. Plasmas **20**, 056106 (2013).

[15] T. Görler, A. E. White, D. Told, F. Jenko, C. Holland, and T. L. Rhodes, Phys. Plasmas **21**, 122307 (2014).

[16] T. Happel, A. Bañón Navarro, G. D. Conway, C. Angioni, M. Bernert, M. Dunne, E. Fable, B. Geiger, T. Görler, F. Jenko, R. M. McDermott, F. Ryter, U. Stroth, and the ASDEX Upgrade Team, Phys. Plasmas **22**, 032503 (2015).

[17] A. Bañón Navarro, T. Happel, T. Görler, F. Jenko, J. Abiteboul, A. Bustos, H. Doerk, D. Told, and the ASDEX Upgrade Team, Phys. Plasmas **22**, 042513 (2015).

[18] P. C. Liewer, Nucl. Fusion **25**, 543 (1985).

[19] R. H. Kraichnan and D. Montgomery, Rep. Prog. Phys. **43**, 547 (1980).

[20] A. A. Schekochihin, S. C. Cowley, W. Dorland, G. W. Hammett, G. G. Howes, G. G. Plunk, E. Quataert, and T. Tatsuno, Plasma Phys. Control. Fusion **50**, 124024 (2008).

[21] M. Barnes, F. I. Parra, and A. A. Schekochihin, Phys. Rev. Lett. **107**, 115003 (2011).

[22] D. R. Hatch, P. W. Terry, W. M. Nevins, and W. Dorland, Phys. Plasmas **16**, 022311 (2009).

[23] O. D. Gürcan, X. Garbet, P. Hennequin, P. H. Diamond, A. Casati, and G. L. Falchetto, Phys. Rev. Lett. **102**, 255002 (2009).

[24] P. Morel, . D. Grcan, and V. Berionni, Plasma Phys. Control. Fusion **56**, 015002 (2014).

[25] P. W. Terry, A. F. Almagri, G. Fiksel, C. B. Forest, D. R. Hatch, F. Jenko, M. D. Nornberg, S. C. Prager, K. Rahbarnia, Y. Ren, and J. S. Sarff, Phys. Plasmas **19**, 055906 (2012).

[26] V. Bratanov, F. Jenko, D. R. Hatch, and M. Wilczek, Phys. Rev. Lett. **111**, 075001 (2013).

[27] P. W. Terry, M. Greenwald, J.-N. Leboeuf, G. R. McKee, D. R. Mikkelsen, W. M. Nevins, D. E. Newman, D. P. Stotler, Task Group on Verification and Validation, U.S. Burning Plasma Organization, and U.S. Transport Task Force, Phys. Plasmas **15**, 062503 (2008).

[28] G. G. Howes, W. Dorland, S. C. Cowley, G. W. Hammett, E. Quataert, A. A. Schekochihin, and T. Tatsuno, Phys. Rev. Lett. **100**, 065004 (2008).

[29] F. Sahraoui, M. L. Goldstein, P. Robert, and Y. V. Khotyaintsev, Phys. Rev. Lett. **102**, 231102 (2009).

[30] A. A. Schekochihin, S. C. Cowley, W. Dorland, G. W. Hammett, G. G. Howes, E. Quataert, and T. Tatsuno, Astrophys. J. **182**, 310 (2009).

[31] E. Mazzucato, Phys. Rev. Lett. **36**, 792 (1976).

[32] A. Semet, A. Mase, W. A. Peebles, N. C. Luhmann, and S. Zweben, Phys. Rev. Lett. **45**, 445 (1980).

[33] E. Mazzucato, Phys. Rev. Lett. **48**, 1828 (1982).

[34] A. Truc and TFR Group, Plasma Phys. Control. Fusion **26**, 1045 (1984).

[35] T. Crowley and E. Mazzucato, Nucl. Fusion **25**, 507 (1985).

[36] P. Hennequin, R. Sabot, C. Honoré, G. T. Hoang, X. Garbet, A. Truc, C. Fenzi, and A. Quéméneur, Plasma Phys. Control. Fusion **46**, B121 (2004).

[37] E. Z. Gusakov, A. D. Gurchenko, A. B. Altukhov, V. V. Bulanin, L. A. Esipov, M. Y. Kantor, D. V. Kouprienko, S. I. Lashkul, A. V. Petrov, and A. Y. Stepanov, Plasma Phys. Control. Fusion **48**, B443 (2006).

[38] X. L. Zou, T. F. Seak, M. Paume, J. M. Chareau, C. Bottereau, and G. Leclert, *Poloidal Rotation Measurement in Tore Supra by Oblique Reflectometry* (Proc. 4$^{\text{th}}$ International Reflectometry Workshop, Cadarache, France, 1999), report EUR-CEA-FC-1674.

[39] M. Hirsch, E. Holzhauer, J. Baldzuhn, and B. Kurzan, *Doppler Reflectometry for the Investigation of poloidally propagating Density Perturbations* (Proc. 4$^{\text{th}}$ International Reflectometry Workshop, Cadarache, France, 1999), report EUR-CEA-FC-1674.

[40] P. Hennequin, C. Honoré, A. Truc, A. Quéméneur, C. Fenzi-Bonizec, C. Bourdelle, X. Garbet, and G. T. Hoang, Nucl. Fusion **46**, S771 (2006).

[41] C. Tröster, Ph.D. thesis, Ludwig-Maximilians-Universität München, 2008.

[42] T. Happel, T. Estrada, E. Blanco, V. Tribaldos, A. Cappa, and A. Bustos, Rev. Sci. Instrum. **80**, 073502 (2009).

[43] W. A. Peebles, T. L. Rhodes, J. C. Hillesheim, L. Zeng, and C. Wannberg, Rev. Sci. Instrum. **81**, 10D902 (2010).

[44] T. Happel, T. Estrada, E. Blanco, C. Hidalgo, G. D. Conway, U. Stroth, and the TJ-II Team, Phys. Plasmas **18**, 102302 (2011).

[45] L. Vermare, Ö. Gürcan, P. Hennequin, C. Honoré, X. Garbet, J. Giacalone, R. Sabot, and F. Clairet, C. R. Phys. **12**, 115 (2011).

[46] L. Vermare, P. Hennequin, O. D. Gurcan, C. Bourdelle, F. Clairet, X. Garbet, R. Sabot, and the Tore Supra Team, Phys. Plasmas **18**, 012306 (2011).

[47] T. Estrada, E. Ascasbar, E. Blanco, A. Cappa, P. H. Diamond, T. Happel, C. Hidalgo, M. Liniers, B. P. van Milligen, I. Pastor, D. Tafalla, and the TJ-II Team, Plasma Phys. Control. Fusion **54**, 124024 (2012).

[48] L. Schmitz, C. Holland, T. L. Rhodes, G. Wang, L. Zeng, A. E. White, J. C. Hillesheim, W. A. Peebles, S. P. Smith, R. Prater, G. R. McKee, Z. Yan, W. M. Solomon, K. H. Burrell, C. T. Holcomb, E. J. Doyle, J. C. DeBoo, M. E. Austin, J. S. deGrassie, and C. C. Petty, Nucl. Fusion **52**, 023003 (2012).

[49] T. Tokuzawa, A. Ejiri, K. Kawahata, K. Tanaka, I. Yamada, M. Yoshinuma, K. Ida, and C. Suzuki, Rev. Sci. Instrum. **83**, 10E322 (2012).

[50] F. Fernández-Marina, T. Estrada, and E. Blanco, Nucl. Fusion **54**, 072001 (2014).

[51] J. C. Hillesheim, N. A. Crocker, W. A. Peebles, H. Meyer, A. Meakins, A. R. Field, D. Dunai, M. Carr, N. Hawkes, and the MAST Team, Nucl. Fusion **55**, 073024 (2015).

[52] U. Stroth, A. B. Navarro, G. Conway, T. Görler, T. Happel, P. Hennequin, C. Lechte, P. Manz, P. Simon, A. Biancalani, E. Blanco, C. Bottereau, F. Clairet, S. Coda, T. Eibert, T. Estrada, A. Fasoli, L. Guimarais, Ö. D. Gürcan, Z. Huang, F. Jenko, W. Kasparek, C. Koenen, A. Krämer-Flecken, M. Manso, A. Medvedeva, D. Molina, V. Nikolaeva, B. Plaum, L. Porte, D. Prisiazhniuk, T. Ribeiro, B. Scott, U. Siart, A. Storelli, L. Vermare, and S. Wolf, Nucl. Fusion **55**, 083027 (2015).

[53] L. Schmitz, D. P. Fulton, E. Ruskov, C. Lau, B. H. Deng, T. Tajima, M. W. Binderbauer, I. Holod, Z. Lin, H. Gota, M. Tuszewski, S. A. Dettrick, and L. C. Steinhauer, Nat. Commun. **7**, 13860 (2016).

[54] E. Z. Gusakov and A. Y. Popov, Plasma Phys. Control. Fusion **46**, 1393 (2004).

[55] J. R. Pinzón, T. Happel, E. Blanco, G. D. Conway, T. Estrada, and U. Stroth, Plasma Phys. Control. Fusion **59**, 035005 (2017).

[56] F. da Silva, S. Heuraux, N. Lemoine, C. Honoré, P. Hennequin, M. Manso, and R. Sabot, Rev. Sci. Instrum. **75**, 3816 (2004).

[57] E. Blanco, T. Estrada, and J. Sánchez, Plasma Phys. Control. Fusion **48**, 699 (2006).

[58] E. Blanco and T. Estrada, Plasma Phys. Control. Fusion **50**, 095011 (2008).

[59] C. Lechte, IEEE Trans. Plasma Sci. **37**, 1099 (2009).

[60] F. da Silva, S. Heuraux, E. Z. Gusakov, and A. Popov, IEEE Trans. Plasma Sci. **38**, 2144 (2010).

[61] J. C. Hillesheim, C. Holland, L. Schmitz, S. Kubota, T. L. Rhodes, and T. A. Carter, Rev. Sci. Instrum. **83**, 10E331 (2012).

[62] P. Hennequin, L. Vermare, Ö. Gürcan, E. Trier, C. Honoré, C. Bourdelle, A. Casati, R. Dumont, G. Falchetto, X. Garbet, R. Sabot, F. Clairet, and the Tore Supra team, *High k spectra in Tore Supra: experiment, theory and modelling* (US Transport Task Force Meeting, San Diego, CA, USA, 2009).

[63] P. Hennequin, *private communication*.

[64] F. Jenko, W. Dorland, M. Kotschenreuther, and B. N. Rogers, Phys. Plasmas **7**, 1904 (2000).

[65] C. Lechte *et al.*, Plasma Phys. Control. Fusion (2017), *submitted.*

[66] T. Happel, G. D. Conway, W. Kasparek, B. Plaum, C. Lechte, D. Wagner, U. Stroth, and the ASDEX Upgrade Team, *Design of a new Doppler Reflectometer Front End for the ASDEX Upgrade Tokamak* (Proc. 10^{th} International Reflectometry Workshop, Padua, Italy, 2011).

[67] R. Sabot, P. Hennequin, and L. Colas, Fusion Sci. Technol. **56**, 1253 (2009).

[68] M. Hirsch and E. Holzhauer, Plasma Phys. Control. Fusion **46**, 593 (2004).

[69] F. Ryter, R. Fischer, J. Fuchs, T. Happel, R. McDermott, E. Viezzer, E. Wolfrum, L. B. Orte, M. Bernert, A. Burckhart, S. da Graca, B. Kurzan, P. McCarthy, T. Pütterich, W. Suttrop, M. Willensdorfer, and the ASDEX Upgrade Team, Nucl. Fusion **57**, 016004 (2017).

[70] T. Happel, P. Manz, F. Ryter, M. Bernert, M. Dunne, P. Hennequin, A. Hetzenecker, U. Stroth, G. D. Conway, L. Guimarais, C. Honoré, E. Viezzer, and The ASDEX Upgrade Team, Plasma Phys. Control. Fusion **59**, 014004 (2017).

[71] B. Kurzan and H. D. Murmann, Rev. Sci. Instrum. **82**, 103501 (2011).

[72] M. Willensdorfer, E. Wolfrum, R. Fischer, J. Schweinzer, M. Sertoli, B. Sieglin, G. Veres, F. Aumayr, and the ASDEX Upgrade Team, Rev. Sci. Instrum. **83**, 023501 (2012).

[73] E. Poli, A. G. Peeters, and G. V. Pereverzev, Comput. Phys. Commun. **136**, 90 (2001).

[74] W. Suttrop, *Practical limitations to plasma edge electron temperature measurements by radiometry of electron cyclotron emission* (Max-Planck-Institute for Plasma Physics, IPP Report 1/306, Garching, Germany, 1997).

[75] S. Klenge, Ph.D. thesis, Institut für Plasmaforschung, Universität Stuttgart, Germany, 2005.

[76] E. Z. Gusakov and A. Y. Popov, Plasma Phys. Control. Fusion **44**, 2327 (2002).

[77] B. D. Scott, Phys. Plasmas **12**, 062314 (2005).

[78] A. D. Gurchenko, E. Z. Gusakov, D. V. Kouprienko, S. Leerink, A. B. Altukhov, J. A. Heikkinen, S. I. Lashkul, L. A. Esipov, and A. Y. Stepanov, Plasma Phys. Control. Fusion **52**, 035010 (2010).

[79] O. D. Gürcan, P. Hennequin, L. Vermare, X. Garbet, and P. H. Diamond, Plasma Phys. Control. Fusion **52**, 045002 (2010).

[80] A. J. Brizard and T. S. Hahm, Rev. Mod. Phys. **79**, 421 (2007).

[81] M. Kotschenreuther, G. Rewoldt, and W. Tang, Comput. Phys. Commun. **88**, 128 (1995).

[82] J. Candy and R. Waltz, J. Comput. Phys. **186**, 545 (2003).

[83] T.-H. Watanabe and H. Sugama, Nucl. Fusion **46**, 24 (2006).

[84] V. Grandgirard, Y. Sarazin, X. Garbet, G. Dif-Pradalier, P. Ghendrih, N. Crouseilles, G. Latu, E. Sonnendrücker, N. Besse, and P. Bertrand, Commun. Nonlinear Sci. Numer. Simul. **13**, 81 (2008).

[85] A. Peeters, Y. Camenen, F. Casson, W. Hornsby, A. Snodin, D. Strintzi, and G. Szepesi, Comput. Phys. Commun. **180**, 2650 (2009).

[86] M. Nunami, T.-H. Watanabe, and H. Sugama, Plasma Fus. Res. **5**, 016 (2010).

[87] P. J. McCarthy, P. Martin, and W. Schneider, *The CLISTE interpretive equilibrium code* (Max-Planck-Institute for Plasma Physics, IPP Report 5/85, Garching, Germany, 1999).

[88] P. Xanthopoulos and F. Jenko, Phys. Plasmas **13**, 092301 (2006).

[89] A. Bañón Navarro, B. Teaca, F. Jenko, G. W. Hammett, T. Happel, and the ASDEX Upgrade Team, Phys. Plasmas **21**, 032304 (2014).

[90] E. Z. Gusakov, M. A. Irzak, and A. Y. Popov, Plasma Phys. Control. Fusion **56**, 025009 (2014).

[91] E. Z. Gusakov, M. A. Irzak, A. Y. Popov, and N. V. Teplova, Plasma Phys. Control. Fusion **57**, 075009 (2015).

[92] E. Z. Gusakov, A. V. Surkov, and A. Y. Popov, Plasma Phys. Control. Fusion **47**, 959 (2005).